Brazilian Journal of Physics
https://doi.org/10.1007/s13538-019-00714-0

CONDENSED MATTER

Synthesis of Magnetite Nanoparticles of Different Size and Shape by Interplay of Two Different Surfactants

Vinícius Mariani Lenart[1] · Rozane de Fátima Turchiello[1] · Maria Pilar Calatayud[2] · Gerardo Fabián Goya[2] · Sergio Leonardo Gómez[3]

Received: 5 July 2019 /

Abstract
Given the central role that nanoparticle size and shape play in many fundamental applications for designing functional materials, fine control of the synthesis has been intensively pursued. A simple one-step method for obtaining monodisperse nanoparticles over a large size range with shape control has not yet been reported. Here, we propose a simple method to control the morphology of magnetite nanoparticles by regulating the amount of non-selective binding surfactant by simply altering the ratio of oleylamine and fatty acid. With this approach, we were able to synthesize magnetite nanoparticles with sizes ranging between 6 ± 1 and 176 ± 20 nm and to select between more rounded or faceted shapes.

Keywords Nanoparticle · Magnetite · Thermal decomposition

1 Introduction

The research on synthesis of iron oxide nanoparticles (NPs) is a field of great interest due to the increasing applications in imaging and magnetic hyperthermia [1]. Envisaging biomedical applications, both the average size and the size distribution affect the interaction of NPs with the cell membrane and their intracellular fate [2]. The term monodisperse nanoparticles [3, 4] is generally used to describe samples in which the particle size varies by less than 5%. In addition to size, other factors such as shape also seem to affect cellular uptake [5, 6]. Thus, improvement of the efficiency and specificity of a given application requires a synthesis route in which morphological parameters can be finely controlled. It is also well known that the magnetic, optical, and electrical properties of the NPs depend on their shape and size, which are determined in the formation process of the nanocrystals. The nucleation of small crystals from a solution is classically described by the spontaneous formation of nuclei that may grow larger than a critical size, which is largely determined by the ratio of surface to bulk energy [7, 8]. The proportion of the reactants involved during the synthesis of NPs determine the final particle size, shape, dispersity, and surface chemistry. Diverse techniques and routes have been proposed in the last years to synthesize magnetite iron oxide nanoparticles [9], like sonochemical [10], reverse micelles [11], pyrolysis [12], electrochemical [13], co-precipitation [14], high-temperature reaction [15], and thermal decomposition [16]. Among the different chemical routes reported for the synthesis of magnetic NPs, high-temperature decomposition of organometallic precursors in a supersaturated solution has demonstrated the best outcomes in terms of particle size homogeneity [4]. Within this framework, the classical growth and nucleation theory stipulates that variation in surface energy caused by the amount and/or type of surfactant is a dominant parameter that determines the crystalline phase [17, 18]. Oleylamine (OL) and oleic acid (OA) are some of the most common surfactants in magnetic NP synthesis. Although the employment of just oleylamine as surfactant allied to other reagents allowed to control the shape of some particles like vanadium oxide [19], a mixture of both surfactants, oleic acid and oleylamine, has been shown to be necessary for the formation of magnetite particles. Previous works have shown that spherical magnetite nanoparticles are obtained with the use of an equimolar mixture of OL and OA [20, 21]. Besides

✉ Sergio Leonardo Gómez
sgomez@uepg.br

[1] Physics Department, Federal University of Technology, Ponta Grossa, PR, Brazil

[2] Institute of Nanoscience of Aragón, University of Zaragoza, Zaragoza, Spain

[3] Physics Department, State University of Ponta Grossa, Ponta Grossa, PR, Brazil

Published online: 23 October 2019

Table 1 Relation of the sample labels with their respective quantities of surfactants, shapes, and respective sizes

Sample	Oleic acid (mmol)	Oleylamine (mmol)	Shape	Size (nm)
Q0	8	0	Truncate octahedron	176 ± 20
Q1	8	4	Octahedron	63 ± 7
Q2	8	8	Rhombic dodecahedron	29 ± 5
Q3	8	12	Spherical-like	17 ± 2
Q4	8	16	Spherical-like	6 ± 1

spherical nanoparticles, truncated octahedral-shaped nanoparticles were obtained by varing the molar ratio of oleic acid and oleylamine in a high-temperature reaction and the sizes of the nanoparticles were controlled by adjusting the heating process. Zhang et al. have also showed different nanoparticle morphologies by controlling reaction heating rate [22]. In addition to spherical and truncated octahedral-shaped particles, there were obtained octahedral magnetite particles by oxidation–precipitation method without any surfactant [23] and rhombic dodecahedrals by two-phase interfacial reaction method [24]. Bu et al. argued about a possible OL/OA cooperative-controlled crystallization mechanism (CCM) which results in a tetragonal bipyramid $NaLa(MoO_4)_2$ nanocrystals [25]. During growth, the high-energy facet grows at a higher rate than the low-energy facets; therefore, the fast-growing facets will eventually disappear, resulting in a nanocrystal terminated with low-energy facets [17]. In this paper, we present to our knowledge the first report on the synthesis by the thermal decomposition method of a set of spherical, octahedral, truncated octahedral, and rhombic dodecahedral magnetite nanoparticles finely tuning the ratio OL/OA, whose thermal diffusivity, measured by thermal lens technique, have been published previously [26].

2 Materials and Methods

The magnetic NPs were synthesized via the thermal decomposition method [20, 27]. For the synthesis there were employed 4 mmol of $Fe(acac)_3$ as precursor and 10.4 g

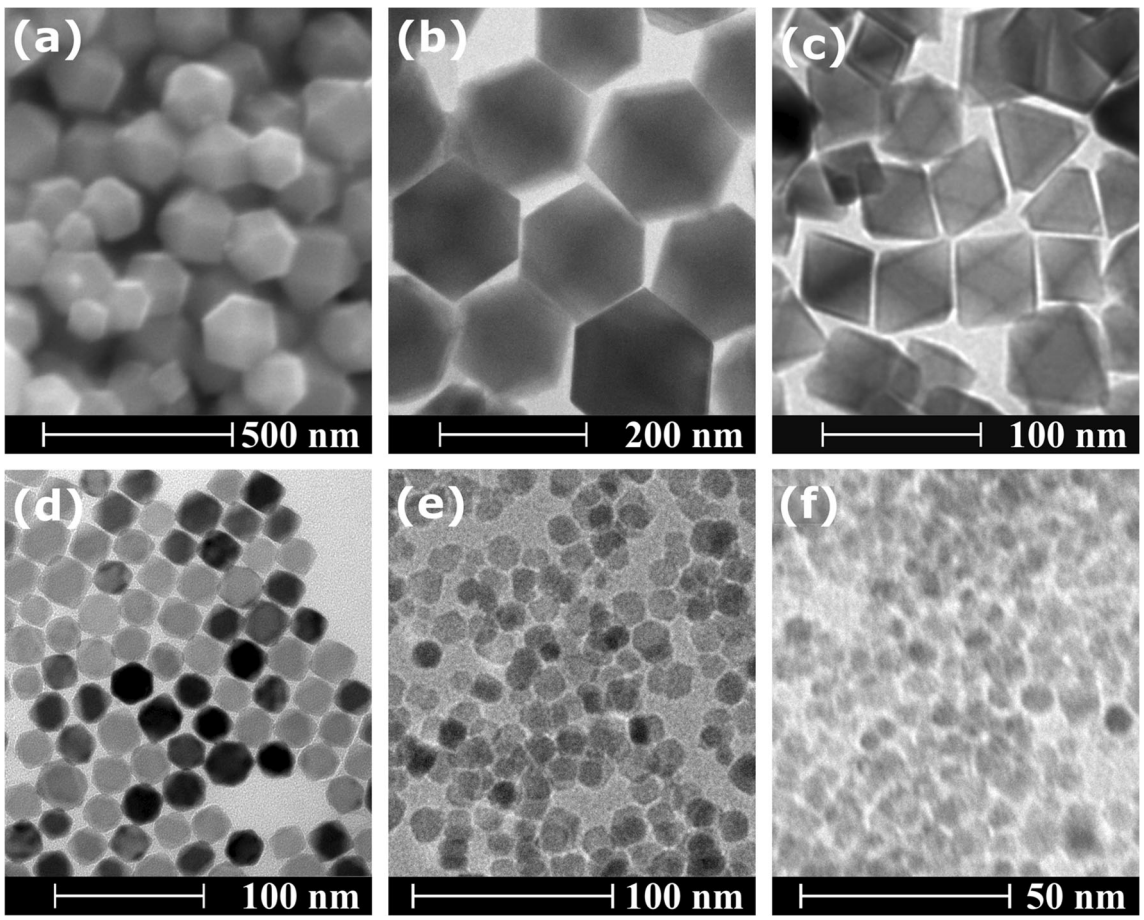

Fig. 1 **a**, **b** Scanning and transmission EM images, respectively, of truncated octahedral (Q0) Fe_3O_4 nanoparticles synthesized without OL with an average size of 176 ± 20 nm. **c**–**f** TEM images of **c** octahedral nanoparticles (Q1) of 63 ± 7 nm, **d** rhombic dodecahedral (Q2) nanoparticles of 29 ± 5 nm, **e** spherical-like nanoparticles (Q3) of 17 ± 2 nm, and **f** spherical-like nanoparticles (Q4) of 6 ± 1 nm

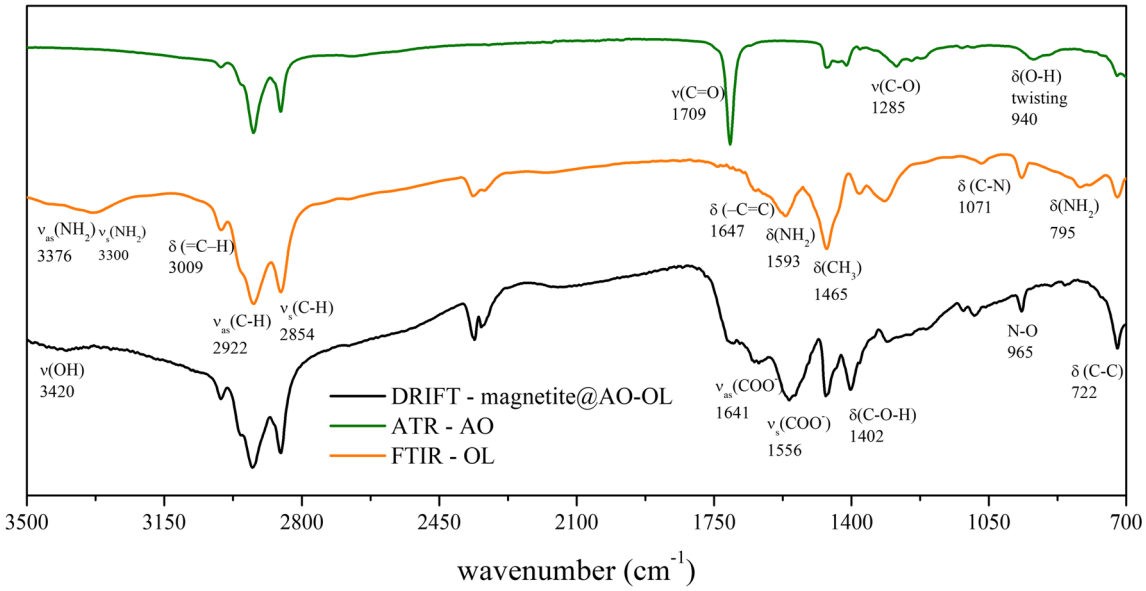

Fig. 2 Fourier transform infrared spectroscopy (FTIR) of OL (yellow line), attenuated total reflection (ATR) of OA (green line), and diffuse reflectance infrared transform (DRIFT) of a sample Q2 (black line). ν_s, symmetric stretching vibration; ν_{as}, asymmetric stretching vibration; δ, bending vibration

of benzyl ether as solvent. The surfactant mixtures as well the sample label set are shown in Table 1. The mixtures were deoxygenated at room temperature for 30 min, heated to 295 °C at a rate of approximately 10 °C/min, maintained at that temperature for 30 min, and then cooled to room temperature. All the one-step synthesis was carried out under nitrogen flow. The product of the synthesis was washed several times with hexane and ethanol and dispersed in hexane. In a second moment, the NPs were dispersed in an aqueous medium following a basic microemulsion process, during which the organic ferrofluid phase was mixed with sodium laurate, water, and NaOH, producing a milky-brown solution with a pH of ≈ 10, which was controlled by the amount of sodium hydroxide. This solution was sonicated and heated to 80 °C to evaporate all of the hexane until the fluid became black. Finally, the particles were washed several times with milli-Q water to remove free molecules or ions. This process coated the particles with a second layer of lauric acid. In order to improve even more the stability, the NPs were dispersed in an aqueous solution of 1% of poly(vinylpyrrolidone) (PVP), which

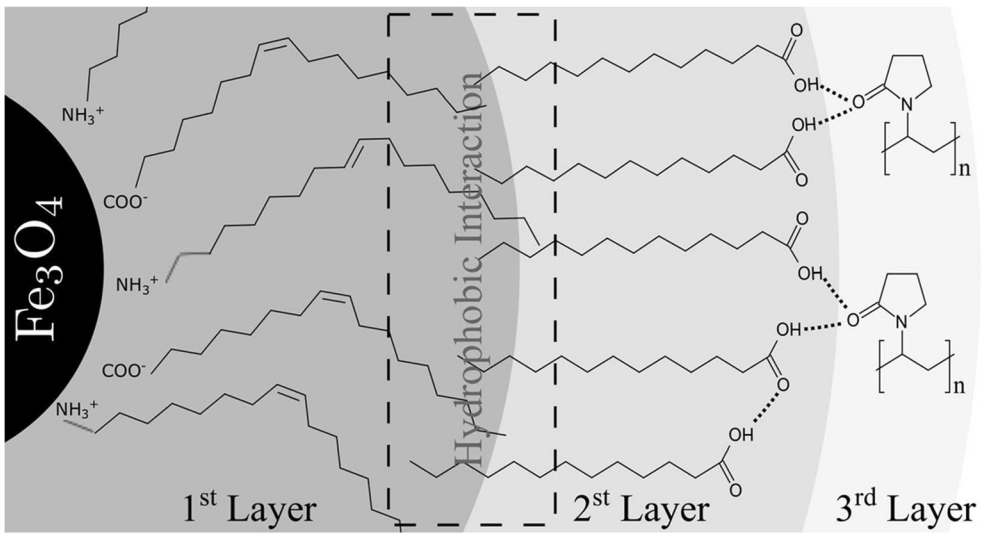

Fig. 3 Schematic representation of the coordination and bonds between surfactants in Fe_3O_4 nanoparticles. The particle is idealized as a smooth sphere; the schematic molecule structures above are not drawn to scale. The dotted lines indicate possible hydrogen bonding. In the first layer, the OL and OA chains are represented along with the likely interactions between the peptide and hydrogen bonds. The second layer is formed by hydrophobic interactions between the carbon chains of the first layer and lauric acid. In the third layer, the amide groups of PVP link to the OH carboxyl groups via hydrogen bonding

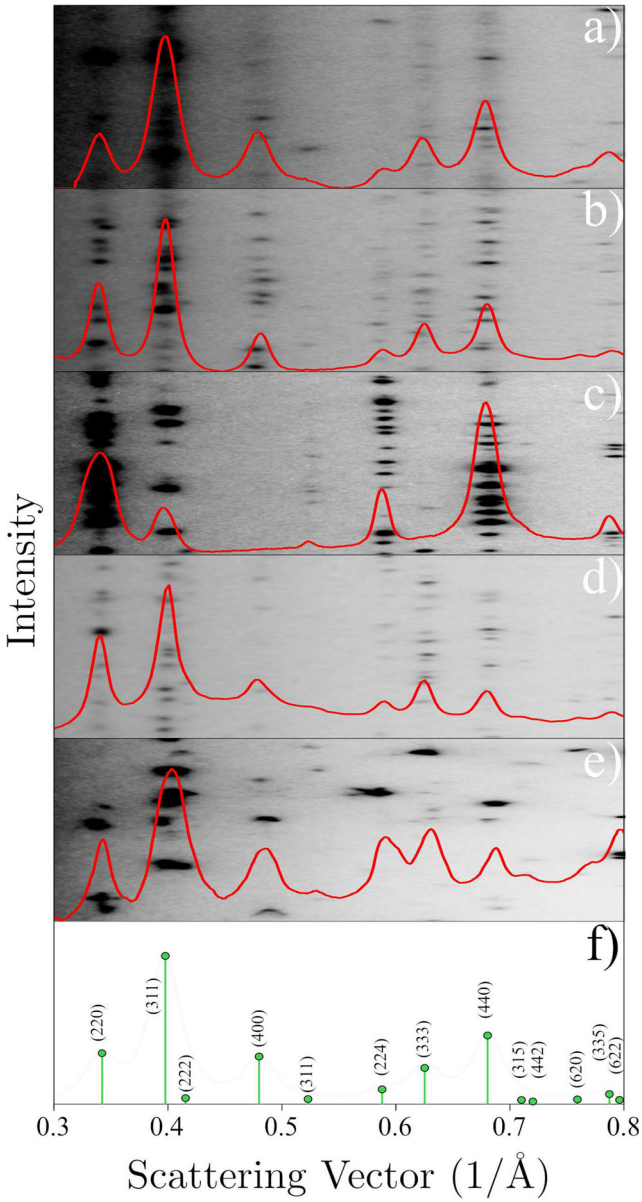

Fig. 4 Electron diffraction pattern of samples. **a** Q4. **b** Q3. **c** Q2. **d** Q1. **e** Q0. **f** The reference [37]

interacts with the carboxyl groups of $C_{12}H_{24}O_2$ to form a third layer [28]. At the end of this process, we obtained ferrofluids in aqueous medium at physiological pH that contained a high concentration of Fe_3O_4 (about 9.9 mg/ml). The zeta potential was measured by Laser Doppler Electrophoresis (ZetaSizer ZS90, Malvern); the morphology and structural phases of the NPs were determined by transmission electron microscopy (TEM), scanning transmission electron microscopy (STEM), and selected area eletron diffraction (SAED), respectively (1200EX-II, JEOL); and the binding form was investigated by infrared (IR) spectroscopy (IRPrestige-21, Shimadzu).

3 Results and Discussion

Figure 1 shows the electron microscope images of the NPs for all the samples described in Table 1. Changing only the quantity of OL, the size was ranged from 6 to 176 nm. Furthermore, the shape changes considerably, which can be correlated with the ratio OL/OA. The zeta potential value for all the samples was about − 44 ± 3 mV, which ensured good stability over a period of 2 years for samples Q0, Q1, and Q2. Due to the size of the samples Q3 and Q4, the attractive forces overcome the steric and ionic repulsion forces, and by gravity effect, they precipitate in a period of 2 months.

Figure 2 shows the IR spectrum of OA, OL, and the sample Q2, obtained by attenuated total reflection (ATR-IR), Fourier transform IR (FTIR), and diffuse reflectance IR transform (DRIFT), respectively. The 1741 cm^{-1} peak assignable to the symmetric stretching vibration of the carbonyl group ν_s(C=O) from the OA shifts to an intense band at about 1641 cm^{-1} for the coated ferromagnetic phase revealing the binding of an OA radical to the magnetite surface. The interaction between the carboxylate head and the metal atom was categorized as being of four possible types: monodentate, bridging (bidentate), chelating (bidentate), and ionic [29]. The separation between the asymmetric and symmetric IR bands of the ion COO^-, ν_{as} and ν_s, respectively, can be used to distinguish the type of interaction between the carboxylate head and the metal atom. In this work, the difference was ascribed to a chelating bidentate type, where the interaction between the COO^- group and the Fe atom was covalent, although the peak at 1709 cm^{-1} in the coated magnetite indicates that some fraction of the OA is bonded to nanoparticle either in monodentate form or as an acid. The 1593 cm^{-1} peak is due to the NH_2 scissoring mode that might be contributing

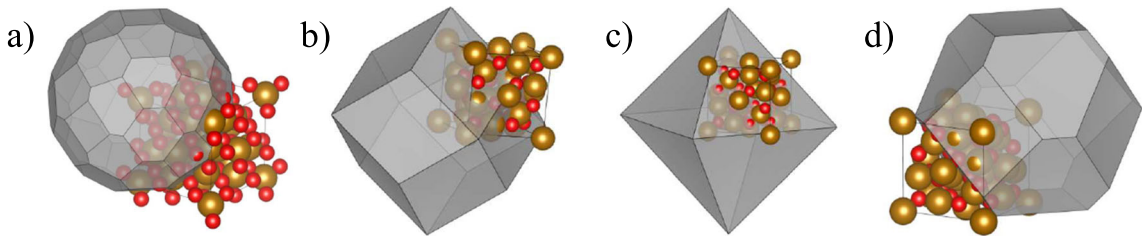

Fig. 5 Simulated magnetite crystal shapes grown with preferential planes. **a** Spherical-like—multiple families. **b** Rhombic dodecahedron—{110}. **c** Octahedron—{111}. **d** truncate octahedron—{100} and {111}

with the symmetric mode of the carboxilate group in the magnetite coated with OA-OL which suggests that the OL is also adsorbed in the surface [30–32]. Similar DRIFT spectra are obtained with the other samples.

The capping agents select and adsorb onto a particular family of crystallographic planes. The carboxylic group of the OA and the amine group of the OL play different roles when binding to the crystal planes: the COO^- groups bind onto the {111} crystal facet, whereas the $-NH_2$ groups undergo weak, unselective binding onto the surface of Fe_3O_4 leading to more spherical particles [33]. A possible cooperative mechanism was described by Bu et al., where OA would deprotonate into carboxylate anions while OL could promote the deprotonation process according to the following process at a specific temperature:

$$C_{17}H_{33}COOH + C_{18}H_{35}NH_2 \rightarrow C_{17}H_{33}COO^- + C_{18}H_{35}NH_3^+ \quad (1)$$

The carboxylate anions could be preferentially and selectively adsorbed onto certain faces because of their higher electron-donating ability as well as the anisotropic character of the crystal nuclei, leading to the growth of uniform crystallographic structures [25]. In the growth of nanocrystals, the high-energy facet grows at a higher rate than the low-energy facets; therefore, the fast-growing facets will eventually disappear, resulting in a nanocrystal terminated with low-energy facets [34, 35]. It is assumed that the commonly used surfactants modify the energy of specific facets through preferential adsorption, influencing the relative growth rate of different facets and thus the shape of a nanocrystal [17]. A possible mechanism for the layer construction and to prevent particle agglomeration through Van der Waals attractive forces and magnetostatic interparticle interactions is illustrated in Fig. 3 [28, 36].

Figure 4 shows the SAED of the samples. The background of the diffractograms shows the 2D image of the diffraction converted to Cartesian coordinates. The red lines are the histogram of the spots diffracted by the planes in which the position pattern matches well with the simulated diffraction of the face centered cubic of magnetite of the reference [37]. Although the intensity of the peaks in different planes changes with the AO/OL ratio used, the intensity peaks in Fig. 4a, b match the reference in Fig. 4f, which is expected for a sample without crystallographic preferred orientation. In Fig. 4c, however, the family {110} is more intense, indicating a different crystal shape. In Fig. 5, we show computer simulations of the crystalline structures obtained by the proposed synthesis. As can be seen in the simple simulation of the crystal shape in the plane {110}, shown in Fig. 5b, it reproduces the same aspect of the nanoparticles seen in Fig. 1d. In Fig. 4d, e, the family {111} is more pronounced than the reference. This is noticeable due to the asymmetry of the main peak caused by the contribution of the plane (222) and by the intensity of the peak referent to the plane (333). This difference is not as explicit in sample Q2, since the electron density of plane (311) is greater than that (111), but smaller than (110). Figure 5 c and d are simulations of crystal shapes in the respective planes (111) and (111) with (100) which agree with TEM images. Evidently, it is not possible to see an apparent difference in the diffraction intensity of the plane (100) in Fig. 4e due to the electron density, yet the simulated shape combines with the final structure of the nanoparticle.

Defining a shape factor parameter υ is as follows:

$$\upsilon \equiv \frac{n_{OL}}{n_{OA}} \quad (2)$$

where n_{OL} and n_{OA} are the number of moles of OL and OA, respectively; we could relate the amount of OA and OL surfactants which bind differently onto crystal facets. When $\upsilon = 0$, the favored direction of growth is the {111} as only OA is present. On the other hand, when OL was added, $\upsilon > 0$, the shape became a mix of cubes and octahedrons, and ultimately spheres as the shape factor increase [7, 17].

The experimental data revealed a simple relationship between the diameter of the NPs and the surfactant/precursor ratio (Fig. 6):

$$d = d_{wo} e^{-6.5\frac{\upsilon}{n_p}}, \quad (3)$$

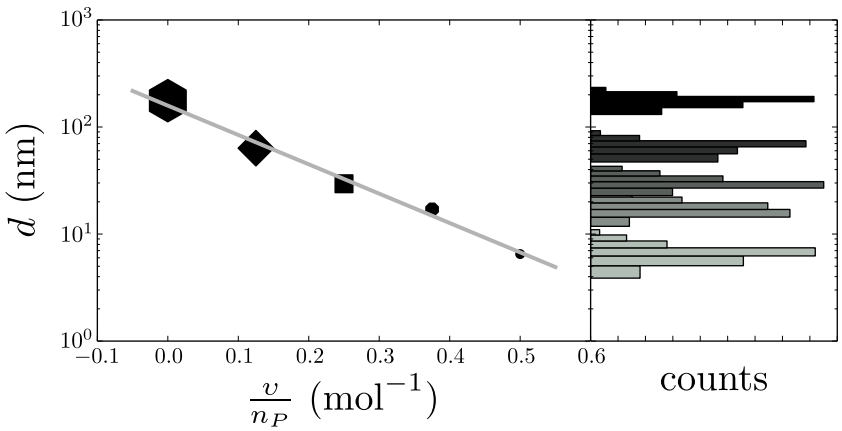

Fig. 6 Dependence of Fe_3O_4 nanoparticle size and shape on the surfactant/precursor ratio. The surfactant contribution is expressed by the shape factor υ defined in Eq. 2. The right panel shows the size distributions of the resulting nanoparticles around the average size. The gray line is the best fit to the experimental data using Eq. 3

where d is the diameter of the NPs, d_{wo} is the diameter of NPs for synthesis without OL, and n_P is the number of moles of precursor. The exponential factor 6.5 was obtained from fitting the experimental data. As predicted in Gibbs free energy for nucleation and growth, surface energy, influenced by the surfactant, is an extremely important parameter in the final size result, as we have seen. However, we found that the concentration of a given surfactant (OL) also acts selectively on the growth of crystallographic planes and shows how the shape changes according to its concentration. It is possible to assume that the same result can be obtained with other methods of synthesis if the energy profile is the same, although the possibility of obtaining this energy profile will depend on the limitations of each method and thermodecomposition seems to be the most appropriate.

4 Conclusions

In summary, we report a very simple and effective way to control both the size and shape of magnetite NPs, solely by modifying the amount and binding specificity of the surfactants involved. The resulting NP size could be adjusted across two orders of magnitude, and furthermore, the final particle shape could be controlled by altering the specificity of the functional groups bonded to the Fe_3O_4 crystal surfaces. The experimental data could be fitted to a simple equation relating the size and morphology of the NPs to the surfactant/precursor ratio using the shape parameter (υ). This simple equation can be used to precisely select a priori both the particle shape and size required for a specific application.

Acknowledgments The authors thank the financial support from MINECO (Spain, project MAT2010-19236), INCT-FCx, and the Brazilian agencies CNPq, CAPES, FAPESP, and Fundação Araucária. V.M. Lenart also acknowledges fellowship from CAPES (Proc. n° 2263-13-0).

Conflict of Interest The authors declare that they have no conflict of interest.

References

1. N. Tran, T.J. Webster, Magnetic nanoparticles: biomedical applications and challenges. J. Mater. Chem. **20**, 8760–8767 (2010)
2. J. Nam, N. Won, J. Bang, H. Jin, J. Park, S. Jung, S. Jung, Y. Park, S. Kim, Surface engineering of inorganic nanoparticles for imaging and therapy. Adv. Drug Deliv. Rev. **65**, 622–648 (2013)
3. J. Park, J. Joo, G.K. Soon, Y. Jang, T. Hyeon, Synthesis of monodisperse spherical nanocrystals. Angew. Chem. Int. Ed. **46**, 4630–4660 (2007)
4. S.G. Kwon, T. Hyeon, Formation mechanisms of uniform nanocrystals via hot-injection and heat-up methods. Small **7**, 2685–2702 (2011)
5. A. Albanese, P.S. Tang, W.C. Chan, The effect of nanoparticle size, shape, and surface chemistry on biological systems. Annu. Rev. Biomed. Eng. **14**, 1–16 (2012)
6. I.A. Wani, T. Ahmad, Size and shape dependant antifungal activity of gold nanoparticles: a case study of candida. Colloid. Surface. B **101**, 162–170 (2013)
7. J. Baumgartner, A. Dey, P.H.H. Bomans, C. Le Coadou, P. Fratzl, N.A.J.M. Sommerdijk, D. Faivre, Nucleation and growth of magnetite from solution. Nat. Mater. **12**, 310–314 (2013)
8. Z. Wu, S. Yang, W. Wu, Shape control of inorganic nanoparticles from solution. Nanoscale **8**, 1237–1259 (2016)
9. S. Laurent, D. Forge, M. Port, A. Roch, C. Robic, L.V. Elst, R.N. Muller, Magnetic iron oxide nanoparticles: synthesis, stabilization, vectorization, physicochemical characterizations, and biological applications. Chem. Rev. **108**, 2064–2110 (2008)
10. E.H. Kim, H.S. Lee, B.K. Kwak, B.K. Kim, Synthesis of ferrouid with magnetic nanoparticles by sonochemical method for MRI contrast agent. J. Magn. Magn. Mater. **289**, 328–330 (2005)
11. Y. Lee, J. Lee, C.J. Bae, J.G. Park, H.J. Noh, J.H. Park, T. Hyeon, Large-scale synthesis of uniform and crystalline magnetite nanoparticles using reverse micelles as nanoreactors under reflux conditions. Adv. Funct. Mater. **15**, 503–509 (2005)
12. R. Strobel, S.E. Pratsinis, Direct synthesis of maghemite, magnetite and wustite nanoparticles by flame spray pyrolysis. Adv. Powder Technol. **20**, 190–194 (2009)
13. L. Cabrera, S. Gutierrez, N. Menendez, M.P. Morales, P. Herrasti, Magnetite nanoparticles: electrochemical synthesis and characterization. Electrochim. Acta **53**, 3436–3441 (2008)
14. I. Nyiro-Kósa, D.C. Nagy, M. Pósfai, Size and shape control of precipitated magnetite nanoparticles. Eur. J. Mineral. **21**(293–302) (2009)
15. K. Parvin, J. Ma, J. Ly, X.C. Sun, D.E. Nikles, K. Sun, L.M. Wang, Synthesis and magnetic properties of monodisperse Fe_3O_4 nanoparticles. J. Appl. Phys. **95**, 7121–7123 (2004)
16. W. W. Yu, J. C. Falkner, C. T. Yavuz, V. L. Colvin, Synthesis of monodisperse iron oxide nanocrystals by thermal decomposition of iron carboxylate salts, Chem. Commun. 2306-2307 (2004)
17. H.-G. Liao, D. Zherebetskyy, H. Xin, C. Czarnik, P. Ercius, H. Elmlund, M. Pan, L.-W. Wang, H. Zheng, Facet development during platinum nanocube growth. Science **345**, 916–919 (2014)
18. W. Wu, Z. Wu, T. Yu, C. Jiang, W.S. Kim, Recent progress on magnetic iron oxide nanoparticles: synthesis, surface functional strategies and biomedical applications. Sci. Technol. Adv. Mater. **16**, 023501 (2015)
19. T.-D. Nguyen, T.-O. Do, Solvo-hydrothermal approach for the shape-selective synthesis of vanadium oxide nanocrystals and their characterization. Langmuir **25**, 5322–5332 (2009)
20. S. Sun, H. Zeng, Size-controlled synthesis of magnetite nanoparticles. J. Am. Chem. Soc. **124**, 8204–8205 (2002)
21. S. Sun, H. Zeng, D.B. Robinson, S. Raoux, P.M. Rice, S.X. Wang, G. Li, Monodisperse MFe_2O_4 (M= Fe, Co, Mn) nanoparticles. J. Am. Chem. Soc. **126**, 273–279 (2004)
22. L. Zhang, Q. Li, S. Liu, M. Ang, M.O. Tade, H.-C. Gu, Synthesis of pyramidal, cubical and truncated octahedral magnetite nanocrystals by controlling reaction heating rate. Adv. Powder Technol. **22**, 532–536 (2011)
23. W. Yu, T. Zhang, J. Zhang, X. Qiao, L. Yang, Y. Liu, The synthesis of octahedral nanoparticles of magnetite. Mater. Lett. **60**, 2998–3001 (2006)
24. X.-L. Cheng, J.-S. Jiang, D.-M. Jiang, Z.-J. Zhao, Synthesis of rhombic dodecahedral Fe3O4 nanocrystals with exposed high-energy 110 facets and their peroxidase-like activity and lithium storage properties. J. Phys. Chem. C **118**, 12588–12598 (2014)
25. W. Bu, Z. Chen, F. Chen, J. Shi, Oleic acid/oleylamine cooperative-controlled crystallization mechanism for monodisperse tetragonal

bipyramid $NaLa(MoO_4)_2$ nanocrystals. J. Phys. Chem. C **113**, 12176–12185 (2009)
26. V.M. Lenart, N.G.C. Astrath, R.F. Turchiello, G.F. Goya, S.L. Gómez, Thermal diffusivity of ferrofluids as a function of particle size determined using the mode-mismatched dual-beam thermal lens technique. J. Appl. Phys. **123**, 085107 (2018)
27. D. Kim, N. Lee, M. Park, B.H. Kim, K. An, T. Hyeon, Synthesis of uniform ferrimagnetic magnetite nanocubes. J. Am. Chem. Soc. **131**, 454–455 (2009)
28. C. Pradip, P. Maltesh, R.A. Somasundaran, S. Kulkarni, Gundiah, Polymer-polymer complexation in dilute aqueous solutions: poly(-acrylic acid)-poly(ethylene oxide) and poly(acrylic acid)-poly(vinylpyrrolidone). Langmuir **7**, 2108–2111 (1991)
29. L. Zhang, R. He, H.-C. Gu, Oleic acid coating on the monodisperse magnetite nanoparticles. Appl. Surf. Sci. **253**, 2611–2617 (2006)
30. M. Klokkenburg, J. Hilhorst, B. Erné, Surface analysis of magnetite nanoparticles in cyclohexane solutions of oleic acid and oleylamine. Vib. Spectrosc. **43**, 243–248 (2007)
31. Z. Xu, C. Shen, Y. Hou, H. Gao, S. Sun, Oleylamine as both reducing agent and stabilizer in a facile synthesis of magnetite nanoparticles. Chem. Mater. **21**, 1778–1780 (2009)
32. S. Mourdikoudis, L.M. Liz-Marzán, Oleylamine in nanoparticle synthesis. Chem. Mater. **25**, 1465–1476 (2013)
33. H. Yang, T. Ogawa, D. Hasegawa, M. Takahashi, Synthesis and magnetic properties of monodisperse magnetite nanocubes. J. Appl. Phys. **103**, 07D526 (2008)
34. A.R. Tao, S. Habas, P. Yang, Shape control of colloidal metal nanocrystals. Small **4**, 310–325 (2008)
35. K. Chen, C. Sun, D. Xue, Morphology engineering of high performance binary oxide electrodes. Phys. Chem. Chem. Phys. **17**, 732–750 (2015)
36. T. Otsuka, Y. Chujo, Preparation and characterization of poly(vinylpyrrolidone)/zirconium oxide hybrids by using inorganic nanocrystals. Polym. J. **40**, 1157–1163 (2008)
37. W. Bragg, The structure of magnetite and the spinels. Nature **95**, 561 (1915)